Acta Cryst. (1996). A**52**, 152–157

A Method of Electron Diffraction Intensity Correction in Combination with High-Resolution Electron Microscopy†

D. X. HUANG,[a] W. LIU,[a] Y. X. GU,[a] J. W. XIONG,[b] H. F. FAN[a] AND F. H. LI[a]*

[a]*Institute of Physics, Chinese Academy of Sciences, Beijing 100080, People's Republic of China, and* [b]*National Laboratory of High Temperature Superconductivity, Institute of Physics, Chinese Academy of Sciences, Beijing 100080, People's Republic of China. E-mail: lifh@aphy01.iphy.ac.cn*

(*Received 5 May 1995; accepted 11 September 1995*)

Abstract

An empirical method is proposed for partially correcting the distortion of electron diffraction intensity caused by Ewald-sphere curvature, crystal bending, thickness inhomogeneity *etc.* The method is based on the combination of electron diffraction and high-resolution electron microscopy. It has been tested with a crystal of high-temperature superconducting oxide $YBa_2Cu_3O_{7-x}$ and shown to be effective.

1. Introduction

There is a long history of the use of electron diffraction as an independent tool to determine crystal structures (Cowley, 1953; Vainshtein, 1964; Zvyagin, 1967). Recently, more attention has been paid to electron diffraction analysis, not only based on various trial-and-error approaches (Dorset, 1985; Brisse, 1989; Zvyagin, 1993), but also on the so-called 'direct phasing method' (Fan *et al.*, 1991; Dorset, 1993; Mo *et al.*, 1992; Gilmore, Shankland & Bricogne, 1993). In addition, electron-diffraction analysis was combined with high-resolution electron microscopy (HREM) to determine crystal structure (Unwin & Henderson, 1975; Ishizuka, Miyazaki & Uyeda, 1982; Fan, Zhong, Zheng & Li, 1985; Hu, Li & Fan, 1992; Dong *et al.*, 1992; Fu *et al.*, 1994). In all cases, the reliability of crystal structure determination is based on the kinematical diffraction approximation. However, for this purpose one often faces many difficulties. The dynamical nature of electron scattering is one of the most essential problems. The dynamical scattering effect is reduced for crystals consisting of light atoms, *e.g.* organic materials. One can also expect to reduce the dynamical scattering effect by working with an ultra high voltage electron microscope (Dorset, Tivol & Turner, 1991; Tivol, Dorset, McCourt & Turner, 1993). Hu, Li & Fan (1992) tried to decrease the dynamical scattering effect with a method similar to the Wilson statistics technique developed in X-ray crystallography (Wilson, 1949). Sha, Fan & Li (1993) proposed a method to correct the dynamical electron scattering effect. A rough structure is first obtained from the experimental electron diffraction data and then the diffraction data are corrected based on the crystal thickness estimated from the rough structure by means of the multislice calculation. Things may not be straightforward even for pure kinematical diffraction. For a thin flat crystal lying perpendicular to the incident beam and having an uniform thickness t, the diffraction intensity is given by

$$I(\mathbf{H}) = |F(\mathbf{H})|^2[\sin^2(\pi ts)]/\pi^2 s^2, \qquad (1)$$

where $F(\mathbf{H})$ denotes the structure factor and s the excitation error. The multiplier of $|F(\mathbf{H})|$ originates from the Ewald-sphere curvature and the Fourier transform of the crystal-shape function. A method to estimate the crystal thickness and to restore structure factors from the electron diffraction intensity was proposed based on the kinematical theory (Tang, Jassen, Zandbergen & Schenk, 1995). Generally, the crystal is not perfectly flat and the crystal thickness is not a constant over the examined area. This leads to the difficulty in accurately determining the structure factors from the observed diffraction intensity.

An approximation of the Ewald sphere as a plan is more or less close to the truth for a bent crystal and for a very small electron wavelength. The structure distortion due to the electron irradiation may lead to a reduction in the diffraction intensity, especially for reflexions in the high-scattering-angle region. Various kinds of structure distortions occur in the same electron diffraction pattern and it can be difficult to distinguish them. Therefore, it is worth developing an empirical method to correct all kinds of distortion at the same time. This is the goal of the present paper, and here a method is proposed on the basis of the combination of electron diffraction and HREM.

A crystal of high-temperature superconducting oxide $YBa_2Cu_3O_{7-x}$ was employed to test the method. It belongs to the orthorhombic system with space group *Pmmm*. The lattice parameters are $a = 3.8177$, $b = 3.8836$ and $c = 11.6872$ Å (Francois *et al.*, 1988).

† This project is partially supported by the National Natural Science Foundation of China.

2. Method

The method is based on the following facts. It is easy to take high-resolution electron-microscope images from a very thin area of sample. However, electron diffraction patterns are usually taken from a larger area with an average thickness bigger than that used for images. Hence, the dynamical scattering effect is usually smaller from images than for diffraction patterns. The key point of the method is to correct the electron diffraction intensity by means of the structural information afforded by an image. When the crystal thickness is below its critical value, the sample can be treated as a pseudo-weak-phase object (Li & Tang, 1985) and some of the atoms, especially heavy atoms, appear black in the optimum defocus image, which is taken near the Scherzer defocus condition (Scherzer, 1949). Such a case is general in experiments. In addition, one can always transform a single image taken under an arbitrary defocus condition into the structure image by image deconvolution (Han, Fan & Li, 1986; Tang & Li, 1988; Hu & Li, 1991). Generally, heavy atoms can be seen more or less clearly in the deconvoluted image of resolution about 2 Å. Because the scattering power of heavy atoms is larger than that of light atoms, the partial structure factors that are calculated by considering merely heavy atoms found in the deconvoluted image are good approximations to the true structure factors. They do not depend on crystal thickness, dynamical scattering effect, crystal bending and other structure distortions. Therefore, the partial structure factors calculated from atoms seen in the deconvoluted images, in most cases only from heavy atoms, can serve as the basis of electron-diffraction-intensity correction.

Divide the reciprocal space into a number of circular zones and denote the average square of the structure-factor modulus inside the ith zone as $\langle|F(\mathbf{H})|^2\rangle_{H_i\pm\Delta H_i}$, where $F(\mathbf{H})$ is the structure factor, H_i the average of H in the ith zone, ΔH_i the half-width of the ith zone and $\langle\ \rangle$ the symbol for averaging. Similar to the treatment of Wilson (1949), we assume that

$$I_c(\mathbf{H})|_{H_i\pm\Delta H_i} = k_{H_i} I_o(\mathbf{H}) \tag{2}$$

with

$$k_{H_i} = \langle|F_p(\mathbf{H})|^2\rangle_{H_i\pm\Delta H_i}/\langle I_o(\mathbf{H})\rangle_{H_i\pm\Delta H_i}, \tag{3}$$

where $I_c(\mathbf{H})|_{H_i\pm\Delta H_i}$ denotes the corrected electron diffraction intensity of a reflexion within the ith zone, $F_p(\mathbf{H})$ denotes the partial structure factor including only the contributions of atoms seen in the deconvoluted image and $I_o(\mathbf{H})$ is the corresponding observed intensity. The coefficient k_{H_i} will be different for different zones.

After correcting the diffraction intensity of reflections in each zone, the phase extension (Fan *et al.*, 1985; Fan, Xiang, Li, Qing, Uyeda & Fujiyoshi, 1991; Hu, Li & Fan, 1992) is carried out by combining the deconvoluted image and $I_c(\mathbf{H})$. Some additional atoms can be seen on the Fourier transform of structure factors obtained after phase extension or on the improved image with enhanced resolution to about 1 Å. A series of improved partial structure factors $F'_p(\mathbf{H})$ can then be calculated by including the additional atoms. Thus, the diffraction intensities can be corrected further by using the formula

$$I'_c(\mathbf{H})|_{H_i\pm\Delta H_i} = k'_{H_i} I_o(\mathbf{H}) \tag{4}$$

with

$$k'_{H_i} = \langle|F'_p(\mathbf{H})|^2\rangle_{H_i\pm\Delta H_i}/\langle I_o(\mathbf{H})\rangle_{H_i\pm\Delta H_i}. \tag{5}$$

The procedure is repeated until it converges to a stable result.

3. Experimental

3.1. *Electron-microscope observation*

The crystals of $YBa_2Cu_3O_{7-x}$ were crushed in an agate mortar. The fine fractures were transferred to a copper grid covered with holey carbon film. The HREM observation was carried out with a JEM-4000EX microscope. A series of electron diffraction patterns was taken with an H-9000NA microscope from the same area of the sample but with different exposure times. The image was taken from an area as thin as possible but the diffraction patterns were not taken from a very thin area. The incident electron beam was always parallel to the a axis.

3.2. *Image digitization and diffraction intensity measurement*

A thin area including 30 unit cells ($10\mathbf{b} \times 3\mathbf{c}$) in the printed image (Fig. 1*a*) was digitized with a CCD camera. The digitized image was averaged by summing all 30 unit cells with the space group *Pmmm* taken into consideration to exclude noise and symmetry distortion. The result is shown in Fig. 2(*a*).

The electron diffraction intensity was measured with a Perkin–Elmer PDS microdensitometer from six negatives taken with different exposure times. The electron diffraction pattern is shown in Fig. 1(*b*). Each diffraction spot was measured inside an area containing 40×40 pixels. A density–intensity characteristic curve (D–I) was obtained from the measurement of six negatives. Only those density values that fell in the linear part of the D–I curve were used for calculating the integral diffraction intensity. The background was deduced from the integral intensity point by point for all diffraction peaks.

4. Image deconvolution

Fig. 3(*a*) shows the theoretical map of the projected potential distribution of $YBa_2Cu_3O_{7-x}$ containing struc-

ture details up to 1 Å. Comparison of Fig. 2(*a*) with Fig. 3(*a*) shows that the defocus values of Fig. 2(*a*) is close to the Scherzer defocus (Scherzer, 1949) because the distribution of dark points in Fig. 2(*a*) is coincident with the location of heavy atoms Ba, Y and Cu. This also means that the sample should be a pseudo-weak-phase object. The image simulation indicates that Fig. 2(*a*) corresponds to an underfocus of 360 Å with crystal thickness about 46 Å.

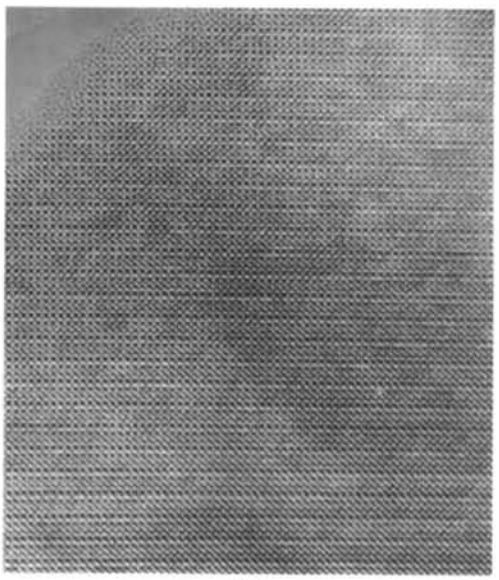

(*a*)

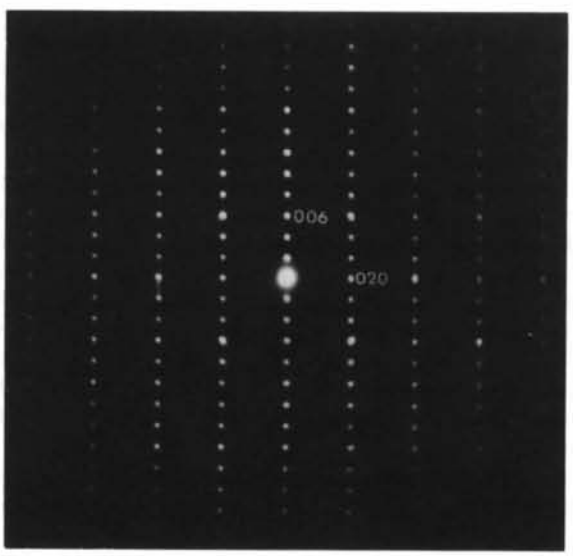

(*b*)

Fig. 1. (*a*) High-resolution electron-microscope image and (*b*) electron diffraction pattern of $YBa_2Cu_3O_{7-x}$ taken with the incident beam parallel to the *a* axis.

The image deconvolution was carried out by means of the method based on the principle of maximum entropy (Hu & Li, 1991) starting from Fig. 2(*a*). The result is shown in Fig. 2(*b*), where Ba, Y and Cu atoms appear with the blackness corresponding to their atomic weight. The inverse Fourier transform of Fig. 2(*b*) yielded 17 independent reflections up to a resolution of about 1.7 Å.

5. Structure distortion from original diffraction intensity

5.1. *Quality of diffraction intensity*

A comparison between the square roots of observed diffraction intensities, $I_o(\mathbf{H})$, and amplitudes of structure factors calculated from the known structure model of

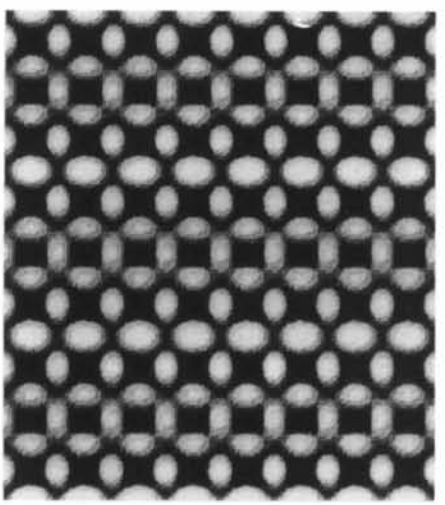

(*a*)

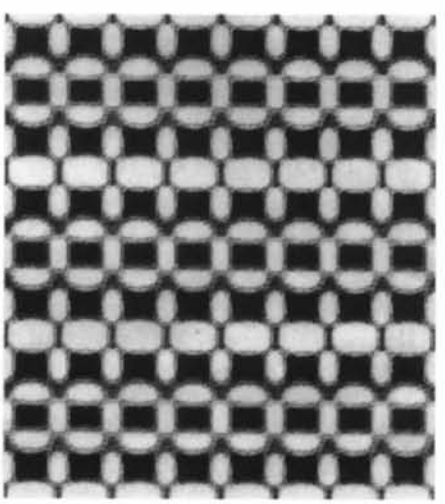

(*b*)

Fig. 2. (*a*) Digitized image from a thin area in Fig. 1(*a*) after removing the noise and the symmetry distortion and (*b*) deconvoluted image from (*a*).

$YBa_2Cu_3O_{7-x}$ (Francois *et al.*, 1988), $F_{cal}(\mathbf{H})$, is given in Table 1. The reliability factor R_o, defined as

$$R_o = \sum \left| [I_o(\mathbf{H})]^{1/2} - |F_{cal}(\mathbf{H})| \right| / \sum |F_{cal}(\mathbf{H})|, \quad (6)$$

which indicates the quality of the observed diffraction intensities, is 0.6346. The map shown in Fig. 3(*b*) was obtained by Fourier transforming the square roots of the observed diffraction intensities at 1 Å together with the

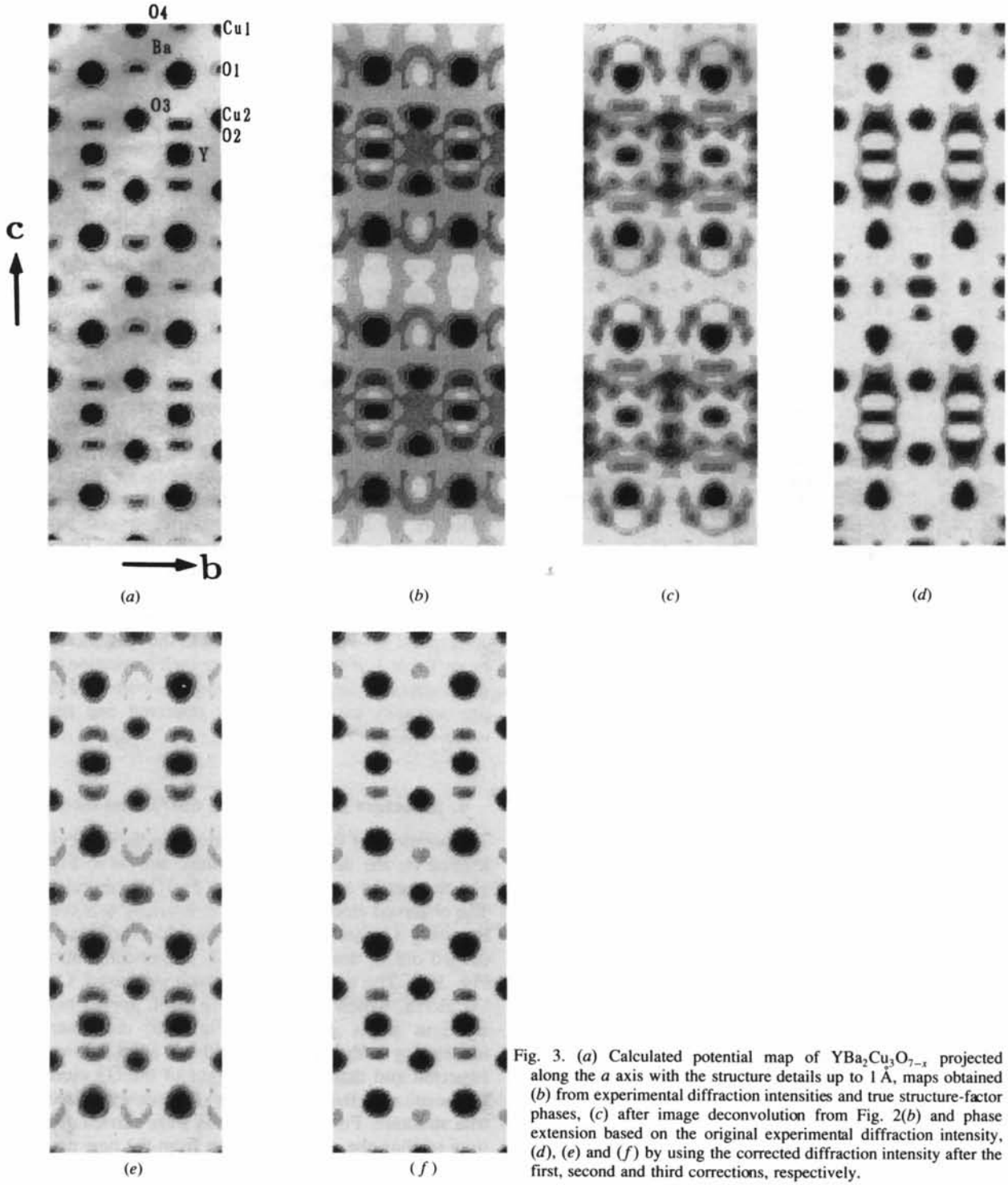

Fig. 3. (*a*) Calculated potential map of $YBa_2Cu_3O_{7-x}$ projected along the *a* axis with the structure details up to 1 Å, maps obtained (*b*) from experimental diffraction intensities and true structure-factor phases, (*c*) after image deconvolution from Fig. 2(*b*) and phase extension based on the original experimental diffraction intensity, (*d*), (*e*) and (*f*) by using the corrected diffraction intensity after the first, second and third corrections, respectively.

Table 1. *Comparison of observed and corrected diffraction intensities*

k	l	$I_o^{1/2}$	$\|F_{cal}\|$	$I_1^{1/2}$	$I_2^{1/2}$	$I_3^{1/2}$
0	1	11.69	1.46	8.54	5.80	4.14
0	2	10.47	5.59	7.27	5.35	3.71
0	3	11.53	12.79	15.10	14.44	12.50
1	0	10.38	14.54	13.11	12.74	11.44
1	1	8.64	1.46	10.31	9.13	7.76
1	2	8.98	4.80	10.28	8.70	7.01
0	4	9.32	5.48	11.79	10.34	9.03
1	3	12.40	26.95	17.02	17.67	18.30
0	5	10.37	19.60	13.94	14.77	16.51
1	4	9.09	10.57	11.89	11.62	11.45
1	5	8.40	3.01	11.18	11.24	11.25
0	6	10.39	25.02	14.09	14.71	15.19
2	0	10.07	35.83	13.78	15.45	16.80
2	1	7.23	1.31	6.78	6.00	5.69
2	2	6.76	1.78	6.31	5.45	5.22
1	6	7.74	4.73	7.52	7.39	7.60
2	3	7.56	4.17	7.54	8.01	8.90
0	7	8.21	9.15	8.27	9.20	10.24
2	4	6.41	4.15	4.97	4.85	4.76
1	7	6.72	3.93	5.41	5.45	5.47
2	5	6.94	13.19	5.73	5.92	5.91
0	8	8.30	4.27	6.85	7.01	7.11
2	6	6.73	17.70	5.48	6.26	6.92
1	8	7.34	9.02	5.95	6.14	6.42
0	9	6.09	5.15	6.19	6.41	6.73
3	0	6.85	3.30	8.27	8.56	8.92
3	1	5.55	0.76	6.77	6.69	6.09
2	7	6.23	6.82	7.80	7.97	7.82
3	2	5.81	1.99	5.87	5.12	4.27
1	9	5.99	7.86	5.98	5.38	4.77
3	3	6.86	13.20	6.90	7.24	7.68
3	4	5.57	5.38	5.59	5.14	4.85
0	10	5.27	4.66	5.35	5.24	5.23
2	8	6.15	3.43	6.52	6.59	6.82
3	5	5.65	1.31	6.04	6.38	6.78
1	10	5.79	9.76	4.88	5.48	6.20
2	9	4.78	5.46	1.91	2.05	2.28
3	6	5.11	2.25	2.14	2.45	2.72
0	11	4.87	10.82	2.05	2.31	2.53
1	11	5.26	0.27	2.29	3.09	3.30
3	7	4.28	2.21	1.97	3.52	5.28
2	10	4.10	3.73	1.66	3.13	3.96

I_o observed diffraction intensity, I_n diffraction intensity after nth correction, F_{cal} structure factor.

phases of structure factors calculated from the structure model of $YBa_2Cu_3O_{7-x}$ (Francois *et al.*, 1988). By comparing this figure with Fig. 3(*a*), it can be seen that all heavy atoms Ba, Y and Cu appear in Fig. 3(*b*) except Cu1. In addition, atoms O3 are revealed at more or less the right positions, O1 are diffuse and O4 are lost. Atoms O2 are superimposed on atoms Cu2 in the projection. Obviously, the original observed diffraction intensities are not adequate for structure analysis.

5.2. *Phase extension with original diffraction intensity*

The phase extension (Fan *et al.*, 1985) was carried out using the *SAPI* program (Fan, Yao, Zheng, Gu & Qian, 1991). Phases of the 17 reflections obtained from the inverse Fourier transform of the deconvoluted image were used as the starting phases. Square roots of the originally measured diffraction intensities up to a resolution of about 1 Å were taken as the amplitudes of the structure factors. At first, the 17 starting phases were kept fixed but were allowed to change in the last two cycles. Phases of 42 reflections at 1 Å resolution were obtained. Fig. 3(*c*) shows the projected potential map calculated with these 42 reflexions. It is far from the true map. The main distortion of the structure is the loss of the Cu1 atoms. Also, all O atoms are either diffuse or split into two or more peaks and many fictitious peaks appear.

5.3. *Difference between observed and corrected diffraction intensities*

From Table 1, it can be seen that on average the observed diffraction intensities are larger than the corrected intensities in the low-angle region. This seems to be due to the curvature of the Ewald sphere. Also, all small structure factors correspond to a high diffraction intensity and most of the large structure factors correspond to a rather low diffraction intensity. This might be due to the dynamical scattering effect. A correction using the above-mentioned method should be effective for removing the influence of the Ewald sphere. The right-most three columns in Table 1 show the corrected diffraction intensities after the first, second and third corrections, I_1, I_2 and I_3, respectively. It is seen that the corrections are effective, and after each correction most of the $I_n^{1/2}$ become closer to the corresponding amplitude of the calculated structure factor. The correction method is therefore effective in removing the influence of Ewald-sphere curvature, crystal bending, crystal-thickness inhomogeneity and structure distortions due to the electron irradiation. It would also be effective to some extent for excluding the dynamical scattering effect if the intensity anomaly pair of reflexions correspond to two different zones in the reciprocal space. From Table 1, it can be seen after each correction that the small structure factors correspond to a corrected diffraction intensity smaller than the observed one and *vice versa*.

6. Structure from corrected diffraction intensity

The positions of Ba, Y and Cu atoms in the unit cell were located on the deconvoluted image shown in Fig. 2(*b*) and the partial structure factors $F_p(\mathbf{H})$ were calculated. The observed electron diffraction intensity was corrected by using (2) and (3). Then, the phase extension was carried out as described in §5.2. The result is shown in Fig. 3(*d*). The map quality is much improved. Cu1 and O4 atoms, which are lost in Fig. 3(*c*), appear here and fictitious peaks existing in Fig. 3(*b*) disappear. The inadequacy is that the peak for the Y atom is lower than expected and that the peak height of the O3 atoms and the position of the O1 atoms deviate somewhat from the true structure. Further corrections were carried out, each time reading the atomic position from the new projected potential map, calculating the new partial structure

factors with a higher approximation and correcting the diffraction intensity by using (4) and (5). Apart from the contribution of Ba, Y and Cu atoms, the contribution of atoms O4 are included in $F'_p(\mathbf{H})$. Such a projected potential map is shown in Fig. 3(*e*) where the peak size of the Y and O3 atoms improves significantly. Although the O1 atoms, which are revealed as sharp peaks in Fig. 3(*d*) turn into diffuse peaks in Fig. 3(*e*), the atomic distance between atoms O1 and Cu1 becomes more reasonable than before. Then the contribution of atoms O1 and O3 is added to calculate $F''_p(\mathbf{H})$. The result is shown in Fig. 3(*f*).

The correction procedure was made iteratively and the result gradually improved (Figs. 3*d* to *f*). But the fourth correction does not lead to an obvious improvement. The reliable factors R_n, defined as

$$R_n = \sum \big||F_n(\mathbf{H})| - |F_{\rm cal}(\mathbf{H})|\big| \Big/ \sum |F_{\rm cal}(\mathbf{H})|, \quad (7)$$

are 0.3088, 0.2229 and 0.1590 after the first, second and third corrections, respectively. Here, $F_n(\mathbf{H})$ denotes the structure factors calculated from the projected potential map obtained after the *n*th correction. A comparison between Fig. 3(*a*) and Fig. 3(*f*) indicates that in Fig. 3(*f*) all atoms appear at the right positions except O1 and the peak height of the atoms changes monotonously with the atomic weight. The distance between atoms O1 and Cu1 is shorter than the normal value. This means that the diffraction intensities were not corrected perfectly.

7. Concluding remarks

Since it is easy to take a high-resolution electron-microscope image at about 2 Å resolution from a thin area of the sample and to transform the image taken at an arbitrary defocus condition to the structure image where atoms appear dark, one can always read the positions of atoms, in most cases all heavy atoms, from the deconvoluted image and then calculate the partial structure factors. The proposed empirical method of diffraction–intensity correction based on these partial structure factors and the image processing technique – image decovolution and phase extension – in HREM is rather effective for excluding the influence of the Ewald sphere and also useful for correcting for the crystal-thickness inhomogeneity, crystal bending and structure distortion due to the electron-beam irradiation. It also seems beneficial in partly removing the dynamical scattering effect. The resolution of the structure map determined by such a method is much higher than that of the optimum defocus image and all atoms can be seen clearly.

References

Brisse, F. (1989). *J. Electron Microsc. Techn.* **11**, 272–279.

Cowley, J. M. (1953). *Acta Cryst.* **6**, 522–529.

Dong, W., Baird, T., Fryer, J. R., MacNicol, D. D., Bricogne, G., Smith, D. J., O'Keefe, M. A. & Hovmöller, S. (1992). *Nature (London)*, **355**, 605–609.

Dorset, D. L. (1985). *J. Electron Microsc. Techn.* **2**, 89–128.

Dorset, D. L. (1993). *Microsc. Soc. Am. Bull.* **23**, 99–108.

Dorset, D. L., Tivol, W. F. & Turner, J. N. (1991). *Ultramicroscopy*, **38**, 41–45.

Fan, H. F., Xiang, S. B., Li, F. H., Qing, P., Uyeda, N. & Fujiyoshi, Y. (1991). *Ultramicroscopy*, **36**, 361–365.

Fan, H. F., Yao, J. X., Zheng, C. D., Gu, Y. X. & Qian, J. Z. (1991). *SAPI-91, a Computer Program for Automatic Solution of Crystal Structures from X-ray Diffraction Data.* Institute of Physics, Chinese Academy of Sciences, Beijing, China.

Fan, H. F., Zhong, Z. Y., Zheng, C. D. & Li, F. H. (1985). *Acta Cryst.* A**41**, 163–165.

Francois, M., Junod, A., Yoon, K., Kewat, A. W., Capponi, J. J., Strobel, P., Marezio, M. & Fischer, P. (1988). *Solid State Commun.* **66**, 117–1125.

Fu, Z. Q., Huang, D. X., Li, F. H., Li, J. Q., Zhao, Z. X., Cheng, T. Z. & Fan, H. F. (1994). *Ultramicroscopy*, **54**, 229–236.

Gilmore, C. J., Shankland, K. & Bricogne, G. (1993). *Proc. R. Soc. London Ser. A*, **442**, 97–111.

Han, F. S., Fan, H. F. & Li, F. H. (1986). *Acta Cryst.* A**42**, 353–356.

Hu, J. J. & Li, F. H. (1991). *Ultramicroscopy*, **35**, 339–350.

Hu, J. J., Li, F. H. & Fan, H. F. (1992). *Ultramicroscopy*, **41**, 387–397.

Ishizuka, K., Miyazaki, M. & Uyeda, N. (1982). *Acta Cryst.* A**38**, 408–413.

Li, F. H. & Tang, D. (1985). *Acta Cryst.* A**41**, 376–382.

Mo, Y. D., Cheng, T. Z., Fan, H. F., Li, J. Q., Sha, B. D., Zheng, C. D., Li, F. H. & Zhao, Z. X. (1992). *Phys. Scr.* T**42**, 18–19.

Scherzer, O. (1949). *J. Appl. Phys.* **20**, 20–29.

Sha, B. D., Fan, H. F. & Li, F. H. (1993). *Acta Cryst.* A**49**, 877–880.

Tang, D., Jansen, J., Zandbergen, H. W. & Schenk, H. (1995). *Acta Cryst.* A**51**, 188–197.

Tang, D. & Li, F. H. (1988). *Ultramicroscopy*, **25**, 61–68.

Tivol, W. F., Dorset, D. L., McCourt, M. P. & Turner, J. N. (1993). *Microsc. Soc. Am. Bull.* **23**, 91–98.

Unwin, P. N. T. & Henderson, R. (1975). *J. Mol. Biol.* **94**, 425–440.

Vainshtein, B. K. (1964). *Structure Analysis by Electron Diffraction.* Oxford: Pergamon Press.

Wilson, A. J. C. (1949). *Acta Cryst.* A**41**, 318–321.

Zvyagin, B. B. (1967). *Electron Diffraction Analysis of Clay Minerals*, pp. 247–280. New York: Plenum Press.

Zvyagin, B. B. (1993). *Microsc. Soc. Am. Bull.* **23**, 68–79.